Journal of Quantitative Spectroscopy & Radiative Transfer 184 (2016) 100–110

Contents lists available at ScienceDirect

Journal of Quantitative Spectroscopy & Radiative Transfer

journal homepage: www.elsevier.com/locate/jqsrt

A global *ab initio* dipole moment surface for methyl chloride

Alec Owens [a,b,*], Sergei N. Yurchenko [a], Andrey Yachmenev [a], Jonathan Tennyson [a], Walter Thiel [b]

[a] Department of Physics and Astronomy, University College London, Gower Street, WC1E 6BT London, United Kingdom
[b] Max-Planck-Institut für Kohlenforschung, Kaiser-Wilhelm-Platz 1, 45470 Mülheim an der Ruhr, Germany

ARTICLE INFO

Article history:
Received 4 May 2016
Received in revised form
12 June 2016
Accepted 27 June 2016
Available online 4 July 2016

Keywords:
Line-lists
Radiative transfer
Databases
HITRAN

ABSTRACT

A new dipole moment surface (DMS) for methyl chloride has been generated at the CCSD(T)/aug-cc-pVQZ(+d for Cl) level of theory. To represent the DMS, a symmetry-adapted analytic representation in terms of nine vibrational coordinates has been developed and implemented. Variational calculations of the infrared spectrum of CH_3Cl show good agreement with a range of experimental results. This includes vibrational transition moments, absolute line intensities of the ν_1, ν_4, ν_5 and $3\nu_6$ bands, and a rotation–vibration line list for both $CH_3{}^{35}Cl$ and $CH_3{}^{37}Cl$ including states up to $J=85$ and vibrational band origins up to 4400 cm^{-1}. Across the spectrum band shape and structure are well reproduced and computed absolute line intensities are comparable with highly accurate experimental measurements for certain fundamental bands. We thus recommend the DMS for future use.

1. Introduction

The proposal of methyl chloride as a potential biosignature gas [1–3] in the search for life outside of the Solar System has ignited interest in its infrared spectrum. There is now considerable motivation for a comprehensive rotation–vibration line list of CH_3Cl. Since methyl chloride is known to contribute to ozone depletion, any such line list would undoubtedly be useful in terrestrial studies. Its importance as an atmospheric molecule is confirmed by the huge number of recent spectroscopic studies [4–31].

The HITRAN database [32] has the most detailed coverage with over 212 000 lines for the two main isotopologues, $^{12}CH_3{}^{35}Cl$ and $^{12}CH_3{}^{37}Cl$ (henceforth labelled as $CH_3{}^{35}Cl$ and $CH_3{}^{37}Cl$). This includes rovibrational transitions up to $J=82$ and covers the 0–3200 cm^{-1} region. However, there are deficiencies and we will see in Section 4.3 that HITRAN is missing a band around 2880 cm^{-1}. Some line positions and intensities are also from theoretical predictions using a fairly old, empirically refined anharmonic force field [33]. Given the numerous high-resolution studies since then, notably in the 3.4 μm region [4] (included in HITRAN2012) and in the 6.9 μm region [14], improvements can be expected in the coverage of CH_3Cl. Another valuable resource is the PNNL spectral library [34] which covers the 600–6500 cm^{-1} region at a resolution of around 0.06 cm^{-1} for temperatures of 5, 25 and 50 °C. Other databases such as GEISA [35] include CH_3Cl but the datasets are not as extensive, whilst the JPL [36] catalogue has been incorporated into HITRAN.

Intensity information is vital for practical applications such as atmospheric modelling or remote sensing. The six fundamental bands of CH_3Cl have all been considered at some stage [4,14,37–50]. Notably, absolute line intensities have been measured for the ν_1, ν_4 and $3\nu_6$ bands in the 2920–3100 cm^{-1} range [4], and for over 900 rovibrational transitions in the ν_5 band [14]. These two studies are the most reliable and complete line intensity measurements for both $CH_3{}^{35}Cl$ and $CH_3{}^{37}Cl$ to date. From a theoretical perspective, calculations of dipole moment derivatives and

* Corresponding author.
E-mail address: alec.owens.13@ucl.ac.uk (A. Owens).

http://dx.doi.org/10.1016/j.jqsrt.2016.06.037
0022-4073/

infrared intensities have been reported [27,33,51–57]. However, we are unaware of any global DMS which could be used for intensity simulations of the rotation–vibration spectrum of CH_3Cl.

Previously we reported [58] two state-of-the-art *ab initio* potential energy surfaces for the two main isotopologues of methyl chloride. Variational calculations of the vibrational $J=0$ energies and equilibrium geometry showed excellent agreement with experimental results. Building on this work, we present a new nine-dimensional *ab initio* DMS which has been computed using high-level electronic structure theory. A symmetrized molecular bond (SMB) representation for XY_3Z-type molecules has been implemented into the nuclear motion code TROVE [59] to represent the DMS analytically. Comprehensive calculations of the rotation–vibration spectrum are then carried out to evaluate the quality of the DMS. The work presented here represents the next step towards generating a complete rovibrational line list applicable for elevated temperatures.

The paper is structured as follows: In Section 2 the electronic structure calculations and analytic representation of the DMS are described. Details of the variational calculations are given in Section 3. In Section 4 the DMS is evaluated against a range of experimental measurements as well as the HITRAN and PNNL spectroscopic databases. Results include vibrational transition moments, absolute line intensities of the ν_1, ν_4, ν_5 and $3\nu_6$ bands, and an overview of the rotation–vibration spectrum for states up to $J=85$ in the 0–6500 cm^{-1} frequency range. Concluding remarks are offered in Section 5.

2. Dipole moment surface

2.1. Electronic structure calculations

The first derivative of the electronic energy with respect to external electric field strength defines the electric dipole moment of a molecule. Working in a Cartesian laboratory-fixed *XYZ* coordinate system with origin at the C nucleus, an external electric field with components ± 0.005 a.u. was applied along each axis and the respective dipole moment component μ_A for $A=X,Y,Z$ determined using finite differences. Calculations were carried out at the CCSD(T) [coupled cluster with all single and double excitations and a perturbational estimate of connected triple excitations] level of theory with the augmented correlation consistent quadruple zeta basis set, aug-cc-pVQZ(+d for Cl) [60–63], in the frozen core approximation. MOLPRO2012 [64] was used for all calculations.

The DMS was evaluated on a nine-dimensional global grid of 44,820 points with energies up to $hc\cdot 50\,000$ cm^{-1} (h is the Planck constant and c is the speed of light). The grid included geometries in the range $1.3\le r_0\le 2.95$ Å, $0.7\le r_i\le 2.45$ Å, $65\le\beta_i\le 165^\circ$ for $i=1,2,3$ and $55\le\tau_{jk}\le 185^\circ$ with $jk=12,13$. Here, the nine internal coordinates are the C–Cl bond length r_0; three C–H bond lengths r_1, r_2 and r_3; three $\angle(H_iCCl)$ interbond angles β_1, β_2 and β_3; and two dihedral angles τ_{12} and τ_{13} between adjacent planes containing H_iCCl and H_jCCl. The grid utilized for the DMS is the same as that used for the PESs previously reported [58].

2.2. Analytic representation

Before fitting an analytic expression to the *ab initio* data it is necessary to establish a suitable molecule-fixed *xyz* coordinate system. Methyl chloride is a prolate symmetric top molecule of the $\boldsymbol{C}_{3v}(M)$ symmetry group [65]. There are six symmetry operations $\{E,(123),(132),(12)^*,(23)^*,(13)^*\}$ which make up $\boldsymbol{C}_{3v}(M)$. The cyclic permutation operation (123) replaces nucleus 1 with nucleus 2, nucleus 2 with nucleus 3, and nucleus 3 with nucleus 1; the permutation-inversion operation (12)* interchanges nuclei 1 and 2 and inverts all particles (including electrons) in the molecular centre of mass; the identity operation E leaves the molecule unchanged. The symmetrized molecular bond (SMB) representation has been successfully applied to molecules of $\boldsymbol{C}_{3v}(M)$ symmetry [66,67] and this approach is employed for the present study.

We first define unit vectors along each of the four bonds of CH_3Cl,

$$\mathbf{e}_i=\frac{\mathbf{r}_i-\mathbf{r}_C}{|\mathbf{r}_i-\mathbf{r}_C|};\quad i=0,1,2,3, \tag{1}$$

where $\mathbf{r}_C$ is the position vector of the C nucleus, $\mathbf{r}_0$ the Cl nucleus, and $\mathbf{r}_1$, $\mathbf{r}_2$ and $\mathbf{r}_3$ the respective H atoms. The *ab initio* dipole moment vector $\boldsymbol{\mu}$ is projected onto the molecular bonds and can be described by molecule-fixed *xyz* dipole moment components,

$$\mu_x=\frac{1}{\sqrt{6}}(2(\boldsymbol{\mu}\cdot\mathbf{e}_1)-(\boldsymbol{\mu}\cdot\mathbf{e}_2)-(\boldsymbol{\mu}\cdot\mathbf{e}_3)), \tag{2}$$

$$\mu_y=\frac{1}{\sqrt{2}}((\boldsymbol{\mu}\cdot\mathbf{e}_2)-(\boldsymbol{\mu}\cdot\mathbf{e}_3)), \tag{3}$$

$$\mu_z=\boldsymbol{\mu}\cdot\mathbf{e}_0. \tag{4}$$

Symmetry-adapted combinations have been formed for μ_x and μ_y and these transform according to E symmetry, while the μ_z component is of A_1 symmetry. The advantage of the SMB representation is that the unit vectors $\mathbf{e}_i$ used to define $\boldsymbol{\mu}$ for any instantaneous positions of the nuclei are related to the internal coordinates only.

To construct the three dipole surfaces corresponding to the components given in Eqs. (2)–(4), a numerical, on-the-fly symmetrization procedure has been implemented. This is similar to the approach employed for the PES [58] but because $\boldsymbol{\mu}$ is a vector quantity we have to consider the transformation properties of the dipole moment components themselves. For μ_z, which points along the C–Cl bond, the process is trivial owing to its A_1 symmetry and invariance to the $\boldsymbol{C}_{3v}(M)$ symmetry operations. Building an analytic expression follows the same steps as the PES. For the two E symmetry components, μ_x and μ_y, the construction is more subtle and they must be treated together.

We consider an initial (reference) term in the dipole expansion belonging to μ_x,

$$\begin{pmatrix}\mu_x\\ \mu_y\end{pmatrix}=\begin{pmatrix}\mu^{\text{initial}}_{x,ijk\ldots}\\ 0\end{pmatrix}, \tag{5}$$

where

$$\mu^{\text{initial}}_{x,ijk\ldots} = \left(\xi_1^i \xi_2^j \xi_3^k \xi_4^l \xi_5^m \xi_6^n \xi_7^p \xi_8^q \xi_9^r\right). \tag{6}$$

This term has maximum expansion order $i+j+k+l+m+n+p+q+r=6$, and is expressed in terms of the nine coordinates,

$$\xi_1 = \left(r_0 - r_0^{\text{ref}}\right), \tag{7}$$

$$\xi_j = \left(r_i - r_1^{\text{ref}}\right); \quad j=2,3,4, \quad i=j-1, \tag{8}$$

$$\xi_k = (\beta_i - \beta^{\text{ref}}); \quad k=5,6,7, \quad i=k-4, \tag{9}$$

$$\xi_8 = \frac{1}{\sqrt{6}}(2\tau_{23} - \tau_{13} - \tau_{12}), \tag{10}$$

$$\xi_9 = \frac{1}{\sqrt{2}}(\tau_{13} - \tau_{12}). \tag{11}$$

Here, $\tau_{23} = 2\pi - \tau_{12} - \tau_{13}$ and the reference structural parameters $r_0^{\text{ref}} = 1.7550$ Å, $r_1^{\text{ref}} = 1.0415$Å and $\beta^{\text{ref}} = 108.414^\circ$. ÅNote that the values of r_0^{ref}, r_1^{ref} and β^{ref} were optimized during the fitting of the DMS.

The action of a symmetry operation $\mathbf{X} = \{E, (123), (132), (12)^*, (23)^*, (13)^*\}$ on Eq. (6) will (i) permute the expansion indices $ijk\ldots$, to $i'j'k'\ldots$ to produce a new expansion term and (ii) permute the unit vectors $\mathbf{e}_i$ for $i=1,2,3$. Using the projection operator technique [65], this latter contribution is projected onto the $\mathbf{e}_x$ and $\mathbf{e}_y$ molecule-fixed vectors and added to the respective dipole moment components. The resulting components, μ'_x and μ'_y, reduce to

$$\begin{pmatrix} \mu'_x \\ \mu'_y \end{pmatrix} = \begin{pmatrix} C_1 \mu^{\mathbf{X}}_{x,ijk\ldots} \\ C_2 \mu^{\mathbf{X}}_{x,ijk\ldots} \end{pmatrix}, \tag{12}$$

where C_1 and C_2 are constants associated with the acting $\boldsymbol{C}_{3v}(M)$ symmetry operation, and $\mu^{\mathbf{X}}_{x,ijk\ldots}$ is the new expansion term connected to Eq. (6) by the symmetry operation $\mathbf{X}$. Note that a contribution arises in μ'_y ($C_2 \neq 0$) due to the projection operator acting on the two-component quantity (μ_x, μ_y).

The steps are repeated for each symmetry operation of $\boldsymbol{C}_{3v}(M)$ and the results summed to produce a final dipole term (ignoring constants),

$$\mu^{\text{final}}_{x,ijk\ldots} = \mu^{E}_{x,ijk\ldots} + \mu^{(123)}_{x,ijk\ldots} + \mu^{(132)}_{x,ijk\ldots} + \mu^{(12)^*}_{x,ijk\ldots} + \mu^{(23)^*}_{x,ijk\ldots} + \mu^{(13)^*}_{x,ijk\ldots}, \tag{13}$$

which is best understood as a sum of symmetrized combinations of different permutations of coordinates ξ_i. Likewise, a similar expression contributes to μ_y. Although we have only considered an initial term belonging to μ_x, the same idea applies to initial terms belonging to μ_y. Incorporating μ_z into the procedure is straightforward, thus enabling the simultaneous construction of all three dipole moment surfaces of CH_3Cl. Each surface is represented by the analytic expression

$$\mu^{\text{total}}_{\alpha}(\xi_1,\xi_2,\xi_3,\xi_4,\xi_5,\xi_6,\xi_7,\xi_8,\xi_9) = \sum_{ijk\ldots} F^{(\alpha)}_{ijk\ldots} \mu^{\text{final}}_{\alpha,ijk\ldots}, \tag{14}$$

where some of the expansion coefficients $F^{(\alpha)}_{ijk\ldots}$ are shared between the x and y components.

A least squares fitting to the *ab initio* data utilizing Watson's robust fitting scheme [68] was employed to determine $F^{(\alpha)}_{ijk\ldots}$ for $\alpha = x, y, z$. Weight factors of the form [69],

$$w_i = \left(\frac{\tanh\left[-0.0006 \times (\tilde{E}_i - 15\,000)\right] + 1.002002002}{2.002002002}\right) \times \frac{1}{N\tilde{E}_i^{(w)}}, \tag{15}$$

were used in the fitting, with normalisation constant $N = 0.0001$ and $\tilde{E}_i^{(w)} = \max(\tilde{E}_i, 10\,000)$, where $\tilde{E}_i$ is the potential energy at the ith geometry above equilibrium (all values in cm^{-1}). At geometries where $r_0 \geq 2.35$ Å, or $r_i \geq 2.00$ Å for $i=1,2,3$, the weights were decreased by several orders of magnitude. This was done because the coupled cluster method is known to become unreliable at very large stretch coordinates, indicated by a T1 diagnostic value > 0.02 [70]. Whilst the energies are not wholly accurate at these points, they ensure that the DMS maintains a reasonable shape towards dissociation.

The three dipole surfaces for μ_x, μ_y and μ_z employed sixth order expansions and used 175, 163 and 235 parameters, respectively. A combined weighted root-mean-square (rms) error of 9×10^{-5} D was obtained for the fitting. Incorporating the analytic representation into variational nuclear motion calculations is relatively straightforward and the implementation requires only a small amount of code. The dipole expansion parameters along with a FORTRAN routine to construct the DMS are provided in the supplementary material.

3. Variational calculations

The nuclear motion program TROVE [59] was employed for all rovibrational calculations and details of the general methodology can be found elsewhere [59,66,71]. Since methyl chloride has already been treated using TROVE [58], we summarize only the key aspects of our calculations.

An automatic differentiation method [71] was used to construct the rovibrational Hamiltonian numerically. The Hamiltonian itself was represented as a power series expansion around the equilibrium geometry in terms of nine vibrational coordinates. The coordinates used are almost identical to those given in Eqs. (7) and (11), except for the potential energy operator where Morse oscillator functions replace the linear expansion variables for stretching modes. In all calculations the kinetic and potential energy operators were truncated at 6th and 8th order, respectively. This level of truncation is adequate for our purposes (see Refs. [59,71] for a discussion of the associated errors of such a scheme). Atomic mass values were employed throughout.

Two purely *ab initio* PESs [58], CBS-35$^{\text{HL}}$ and CBS-37$^{\text{HL}}$, corresponding to the two main isotopologues, $CH_3{}^{35}Cl$ and $CH_3{}^{37}Cl$, have been utilized for the present study. The surfaces are based on extensive explicitly correlated coupled cluster calculations with extrapolation to the

complete basis set (CBS) limit and include a range of additional higher-level energy corrections. The CBS-35^{HL} and CBS-37^{HL} PESs reproduce the fundamental term values with rms errors of 0.75 and 1.00 cm^{-1}, respectively. We are therefore confident that the DMS of CH_3Cl can be evaluated accurately in conjunction with these PESs.

A multi-step contraction scheme [66] is used to construct the vibrational basis set and a polyad number truncation scheme controls its size. For CH_3Cl, we define the polyad number

$$P = n_1 + 2(n_2 + n_3 + n_4) + n_5 + n_6 + n_7 + n_8 + n_9 \le P_{\max}, \quad (16)$$

and this does not exceed a predefined maximum value $P_{\max}$. Here, the quantum numbers n_k for $k = 1, \ldots, 9$ correspond to primitive basis functions ϕ_{n_k} for each vibrational mode. Multiplication with rigid-rotor eigenfunctions $|J, K, m, \tau_{\text{rot}}\rangle$ produces the final symmetrized basis set for use in $J > 0$ calculations. The quantum number K is the projection (in units of $\hbar$) of J onto the molecule-fixed z-axis, whilst τ_{rot} determines the rotational parity as $(-1)^{\tau_{\text{rot}}}$. As we will see in Section 4, different sized basis sets have been utilized in this work and this reflects the computational demands of variational calculations of rovibrational spectra.

TROVE automatically assigns quantum numbers to the eigenvalues and corresponding eigenvectors by analysing the contribution of the basis functions. To be of spectroscopic use we map the vibrational quantum numbers n_k to the normal mode quantum numbers v_k commonly used in spectroscopic studies. For CH_3Cl, vibrational states are labelled as $v_1\nu_1 + v_2\nu_2 + v_3\nu_3 + v_4\nu_4 + v_5\nu_5 + v_6\nu_6$ where v_i counts the level of excitation.

The normal modes of methyl chloride are of A_1 or E symmetry. The three non-degenerate modes have A_1 symmetry; the symmetric CH_3 stretching mode ν_1 (2967.77/2967.75 cm^{-1}), the symmetric CH_3 deformation mode ν_2 (1354.88/1354.69 cm^{-1}) and the C–Cl stretching mode ν_3 (732.84/727.03 cm^{-1}). Whilst the three degenerate modes have E symmetry; the CH_3 stretching mode $\nu_4^{\ell_4}$ (3039.26/3039.63 cm^{-1}), the CH_3 deformation mode $\nu_5^{\ell_5}$ (1452.18/1452.16 cm^{-1}) and the CH_3 rocking mode $\nu_6^{\ell_6}$ (1018.07/1017.68 cm^{-1}). The values in parentheses are the experimentally determined fundamental frequencies for $CH_3{}^{35}Cl/CH_3{}^{37}Cl$ [4,22]. The additional vibrational angular momentum quantum numbers ℓ_4, ℓ_5 and ℓ_6 are necessary to resolve the degeneracy of their respective modes.

4. Results

4.1. Vibrational transition moments

As an initial test of the DMS we compute vibrational transition moments,

$$\mu_{if} = \sqrt{\sum_{\alpha=x,y,z} |\langle \Phi_{\text{vib}}^{(f)} | \overline{\mu}_\alpha | \Phi_{\text{vib}}^{(i)} \rangle|^2}. \quad (17)$$

Here, $|\Phi_{\text{vib}}^{(i)}\rangle$ and $|\Phi_{\text{vib}}^{(f)}\rangle$ are the initial and final state vibrational ($J = 0$) eigenfunctions, respectively, and $\overline{\mu}_\alpha$ is the electronically averaged dipole moment function along the molecule-fixed axis $\alpha = x, y, z$.

Transition moments have been determined experimentally for the six fundamental modes of $CH_3{}^{35}Cl$ and these are listed in Table 1 along with our computed values. Calculations employed a polyad truncation number of $P_{\max} = 12$ which is sufficient for converging μ_{if}. Overall the agreement is encouraging and it indicates that the DMS should be reliable for intensity simulations of the fundamental bands.

For $CH_3{}^{37}Cl$, band strength measurements of the ν_3 [43] and ν_6 [45] bands have been carried out but only minor differences were observed compared to $CH_3{}^{35}Cl$ [40,44]. Likewise, as seen in Table 1 the computed transition moments for the fundamentals only marginally differ compared to $CH_3{}^{35}Cl$. It seems the intensity variation from

Table 1
Calculated vibrational transition moments (in Debye) and frequencies (in cm^{-1}) from the vibrational ground state for $CH_3{}^{35}Cl$ and $CH_3{}^{37}Cl$.

Mode	Sym.	Experiment[a]	Calculated	μ_{if}^{calc}	μ_{if}^{exp}	Ref.
$CH_3{}^{35}Cl$						
ν_1	A_1	2967.77	2969.16	0.05296	0.053[b]	Elkins et al. [41]
ν_2	A_1	1354.88	1355.01	0.05260	0.05006(1)[c]	Blanquet et al. [49]
ν_3	A_1	732.84	733.22	0.11468	0.1121(8)	Dang-Nhu et al. [40]
ν_4	E	3039.26	3038.19	0.03108	0.033[d]	Elkins et al. [41]
ν_5	E	1452.18	1452.56	0.05451	0.0527(7)	Cappellani et al. [42]
ν_6	E	1018.07	1018.05	0.03707	0.0388[e]	Blanquet et al. [44]
$CH_3{}^{37}Cl$						
ν_1	A_1	2967.75	2969.14	0.05296	–	–
ν_2	A_1	1354.69	1354.82	0.05275	–	–
ν_3	A_1	727.03	727.40	0.11416	–	–
ν_4	E	3039.63	3037.71	0.02939	–	–
ν_5	E	1452.16	1452.53	0.05449	–	–
ν_6	E	1017.68	1017.66	0.03724	–	–

[a] From Bray et al. [4] and Nikitin et al. [22].
[b] From Papoušek et al. [56] but derived from band strength measurement of $S_v = 84.3 \pm 3.3$ cm^{-2} atm^{-1} at 296 K [41].
[c] Value of $\mu_{\nu_2}^{\text{exp}} = 0.0473(7)$ D determined in Cappellani et al. [42].
[d] From Papoušek et al. [56] but derived from band strength measurement of $S_v = 33.6 \pm 1.4$ cm^{-2} atm^{-1} at 296 K [41].
[e] From Papoušek et al. [56] but derived from band strength measurement of $S_v = 15.1 \pm 1.6$ cm^{-2} atm^{-1} at 296 K [44].

isotopic substitution in methyl chloride is relatively small and in some instances almost negligible. A list of computed transitions moments from the vibrational ground state for 79 levels up to 4200 cm^{-1} is provided in the supplementary material. Note that for the equilibrium dipole moment of methyl chloride we calculate $\mu = 1.8909$ D which is close to the experimental value of $\mu = 1.8959(15)$ D [72].

4.2. Absolute line intensities of the ν_1, ν_4, ν_5 and $3\nu_6$ bands

Recently, absolute line intensities were determined for the ν_1, ν_4 and $3\nu_6$ bands around the 3.4 μm region [4] (included in HITRAN2012), and for the ν_5 band in the 6.9 μm region [14]. To assess the DMS we compare against these works for both isotopologues up to $J = 15$. Calculating higher rotational excitation is computationally demanding (rovibrational matrices scale linearly with J) so we set $P_{max} = 10$ which is sufficient for reliable intensities. A study on the five-atom molecule SiH_4 [73], which has similar convergence properties with respect to P_{max}, also employed $P_{max} = 10$ to produce intensities of the ν_3 band with an estimated convergence error of 1% or less for transitions up to $J = 16$. Because the two *ab initio* PESs used in this study, CBS-35^{HL} and CBS-37^{HL}, can at best only be considered accurate to about ± 1 cm^{-1}, for illustrative purposes we have shifted computed line positions to better match experiment in the following comparisons.

Absolute absorption intensities have been simulated at room temperature ($T = 296$ K) using the expression,

$$I(f \leftarrow i) = \frac{A_{if}}{8\pi c} g_{ns} \left(2J_f + 1\right) \frac{\exp\left(-E_i/kT\right)}{Q(T)\nu_{if}^2} \left[1 - \exp\left(-\frac{hc\nu_{if}}{kT}\right)\right], \tag{18}$$

where A_{if} is the Einstein A coefficient of a transition with frequency ν_{if} between an initial state with energy E_i, and a final state with rotational quantum number J_f. Here, k is the Boltzmann constant, T is the absolute temperature and c is the speed of light. The nuclear spin statistical weights are $g_{ns} = \{16, 16, 16\}$ for states of symmetry $\{A_1, A_2, E\}$, respectively. These values have been calculated using the method detailed in Jensen and Bunker [74]. For the partition function we use values of $Q(T) = 57,915.728$ and 58,833.711 for $CH_3{}^{35}Cl$ and $CH_3{}^{37}Cl$, respectively [32]. Note that to ensure a correct comparison with the experimental studies of Bray et al. [4] and Barbouchi Ramchani et al. [14], the intensities of overlapping A_1 and A_2 spectral lines (listed as being of A symmetry) must be halved.

In Fig. 1 we plot absolute line intensities for 126 transitions of the ν_1 band and their corresponding residuals $\left(\%\left[\frac{\text{obs}-\text{calc}}{\text{obs}}\right]\right)$ compared to measurements from Bray et al. [4]. The majority of computed intensities, although tending to be marginally stronger, are within the experimental accuracy of 10% or better [75]. Calculated line positions had on average a residual error of $\Delta_{\text{obs}-\text{calc}} = -1.35$ cm^{-1} and this has been corrected for in Fig. 1. Similarly, computed intensities of the ν_4 band shown in Fig. 2 are largely within experimental uncertainty. Here, line positions possessed a residual error of $\Delta_{\text{obs}-\text{calc}} = -1.42$ cm^{-1}.

Line intensities of the $3\nu_6$ band are shown in Fig. 3. Excited modes are harder to converge and the size of the vibrational basis set at $P_{max} = 10$ means the respective rovibrational energy levels have a convergence error of 1.0 cm^{-1} for low J values (compared to errors of ≈ 0.1, 0.5 and 0.03 cm^{-1} for the ν_1, ν_4 and ν_5 bands, respectively). The effect is that computed line intensities will have an uncertainty of around 5%. Even so, the agreement for the 16 lines from Bray et al. [4] is good. Note that line positions displayed a residual error of $\Delta_{\text{obs}-\text{calc}} = -1.23$ cm^{-1}.

A high-resolution study of the ν_5 band measured absolute line intensities with an experimental accuracy of 5% or less, and line positions with an average estimated accuracy between 10^{-3} and 10^{-4} cm^{-1}. As shown in Fig. 4 a significant number of computed line intensities are within experimental uncertainty and agreement for the 256 transitions up to $J = 15$ is excellent. Here calculated line positions had a residual error of $\Delta_{\text{obs}-\text{calc}} = -0.40$ cm^{-1}.

4.3. Overview of rotation–vibration line list

The HITRAN database contains over 212 000 lines for CH_3Cl and considers transitions up to $J = 82$. To compute such highly excited rovibrational energy levels it has been

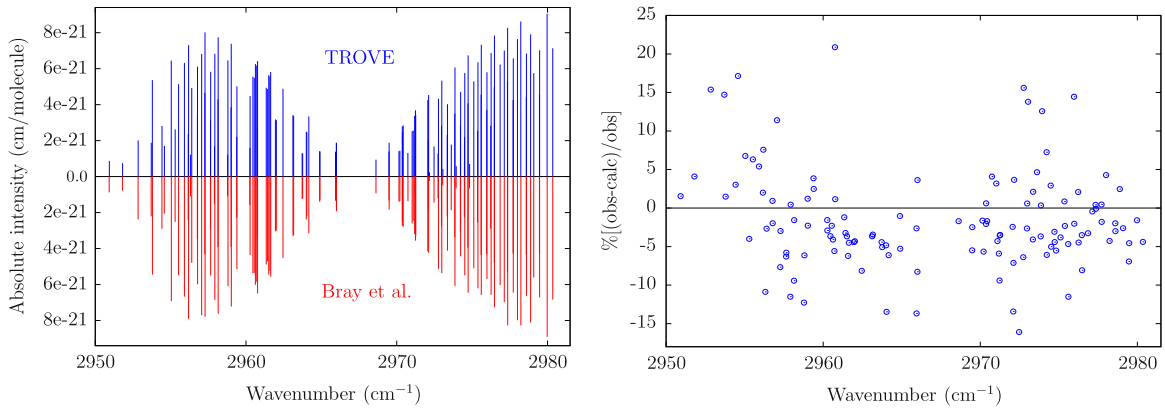

Fig. 1. Absolute line intensities of the ν_1 band for transitions up to $J = 15$ (left) and the corresponding residuals $\left(\%\left[\frac{\text{obs}-\text{calc}}{\text{obs}}\right]\right)$ (right) when compared with measurements from Bray et al. [4]. Transitions for both $CH_3{}^{35}Cl$ and $CH_3{}^{37}Cl$ are shown and the intensities have not been scaled to natural abundance. For illustrative purposes TROVE line positions have been shifted by -1.35 cm^{-1}.

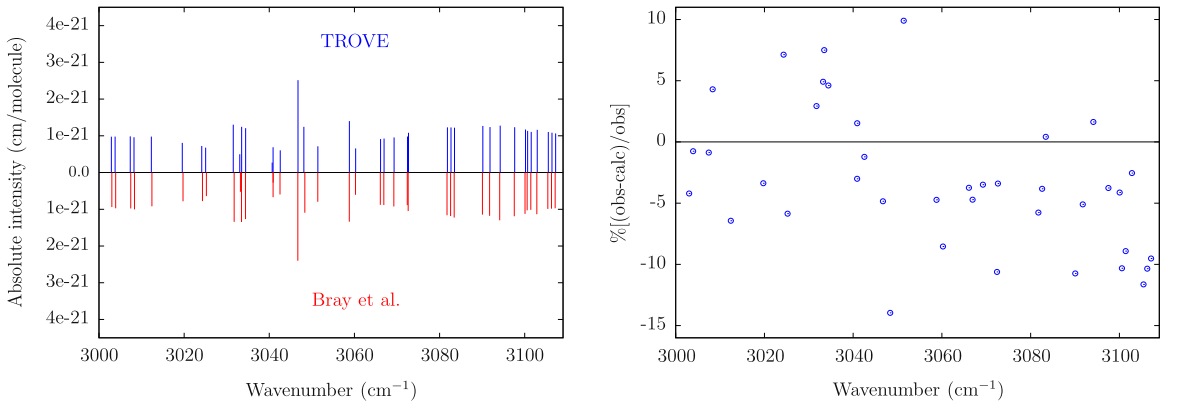

Fig. 2. Absolute line intensities of the ν_4 band for transitions up to $J=15$ (left) and the corresponding residuals $(\%[\frac{\text{obs}-\text{calc}}{\text{obs}}])$ (right) when compared with measurements from Bray et al. [4]. Transitions for both $CH_3{}^{35}Cl$ and $CH_3{}^{37}Cl$ are shown and the intensities have not been scaled to natural abundance. For illustrative purposes TROVE line positions have been shifted by $-1.42\,\text{cm}^{-1}$.

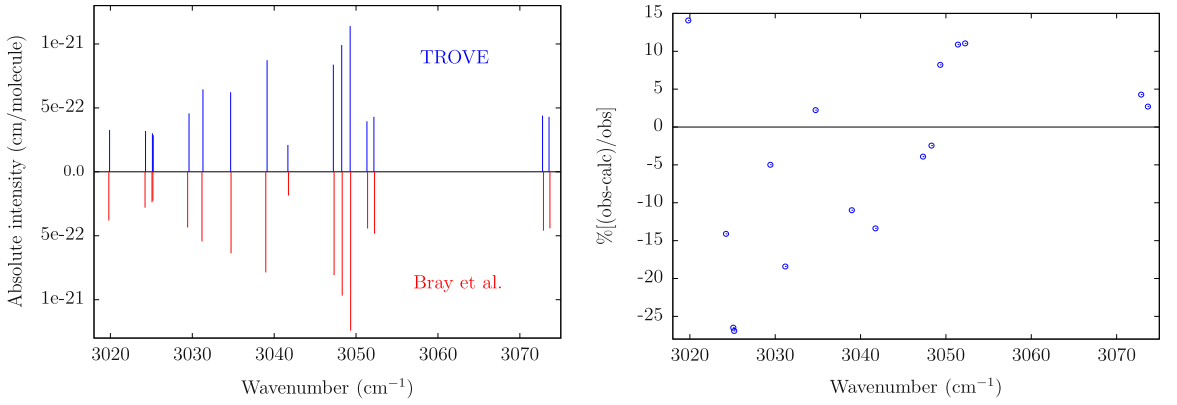

Fig. 3. Absolute line intensities of the $3\nu_6$ band for transitions up to $J=15$ (left) and the corresponding residuals $(\%[\frac{\text{obs}-\text{calc}}{\text{obs}}])$ (right) when compared with measurements from Bray et al. [4]. Transitions for both $CH_3{}^{35}Cl$ and $CH_3{}^{37}Cl$ are shown and the intensities have not been scaled to natural abundance. For illustrative purposes TROVE line positions have been shifted by $-1.23\,\text{cm}^{-1}$.

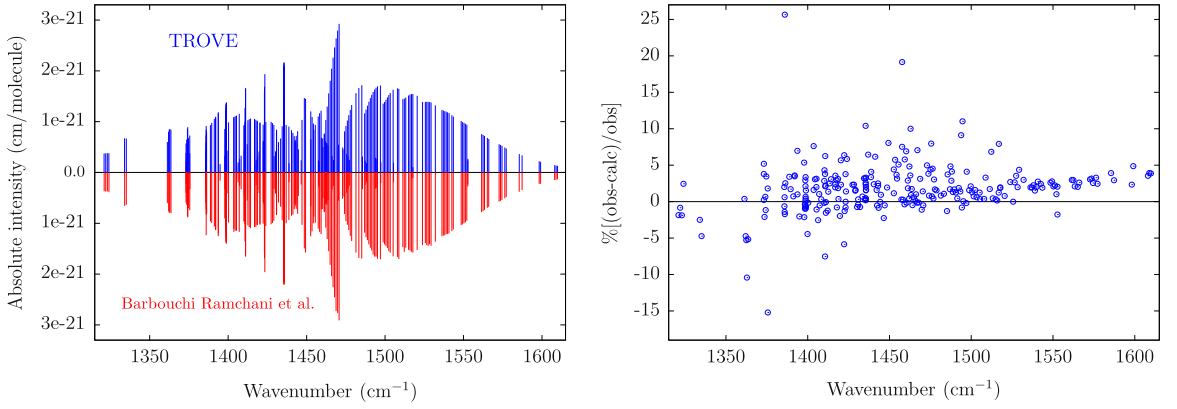

Fig. 4. Absolute line intensities of the ν_5 band for transitions up to $J=15$ (left) and the corresponding residuals $(\%[\frac{\text{obs}-\text{calc}}{\text{obs}}])$ (right) when compared with measurements from Ramchani et al. [14]. Transitions for both $CH_3{}^{35}Cl$ and $CH_3{}^{37}Cl$ are shown and the intensities have not been scaled to natural abundance. For illustrative purposes TROVE line positions have been shifted by $-0.40\,\text{cm}^{-1}$.

necessary to again reduce the size of the vibrational basis set. Calculations were carried out with $P_{\text{max}}=8$ and an upper energy level cut-off of $8000\,\text{cm}^{-1}$. Subsequent transitions and intensities were computed for a $6300\,\text{cm}^{-1}$ frequency window with a lower state energy threshold of $4400\,\text{cm}^{-1}$. Information has undoubtedly been lost by introducing these thresholds but the values were carefully chosen to keep this to a minimum. Such restrictions also allow the straightforward calculation of high J values in a timely manner on compute nodes with

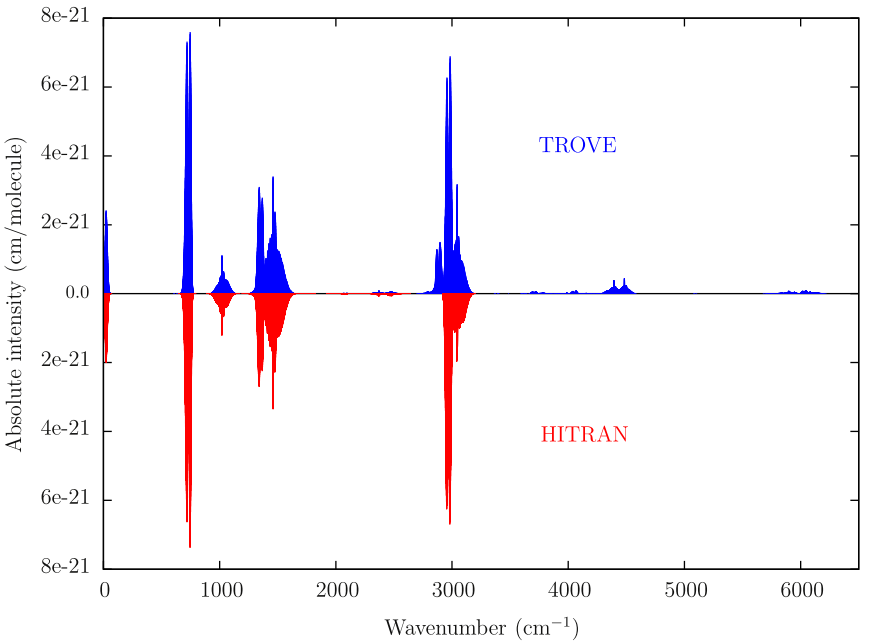

Fig. 5. Overview of methyl chloride rotation–vibration line list up to $J=85$ compared with all transitions in the HITRAN database [32]. Computed intensities have been scaled to natural abundance.

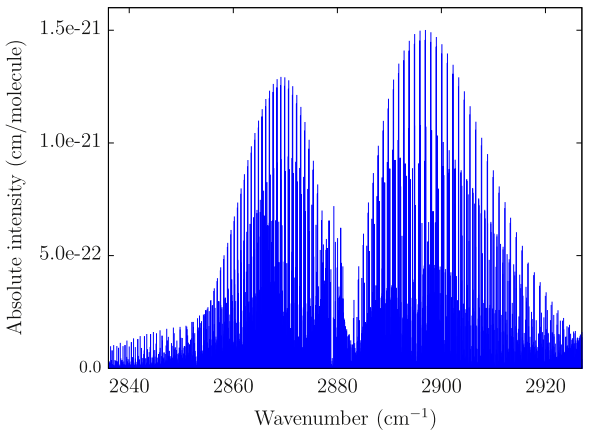

Fig. 6. The $2\nu_5$ band of methyl chloride. Computed intensities have been scaled to natural abundance.

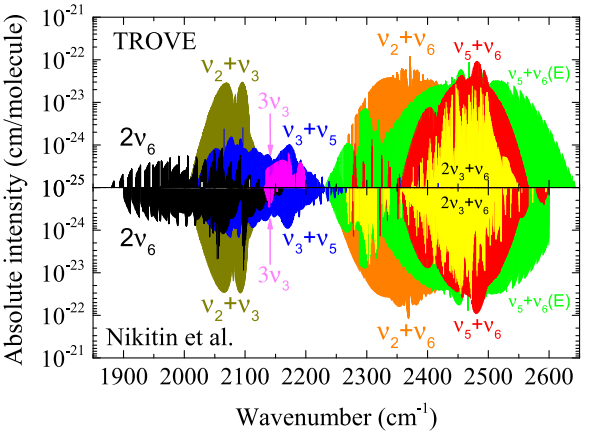

Fig. 7. Absolute line intensities of $CH_3{}^{35}Cl$ in the range 1900–2600 cm^{-1} compared with measurements from Nikitin et al. [23]. Computed TROVE transitions are up to $J=85$ whilst the results from Nikitin et al. [23] are up to $J=47$. Note that a logarithmic scale has been used for the y-axis.

64 GB of RAM. Note that for pure rotational transitions in HITRAN the hyperfine structure has been resolved [76]. Therefore, in order to have a reliable comparison for this spectral region we scale our intensities by a factor of 1/2.

In Fig. 5 we present a computed line list up to $J=85$ for both isotopologues of methyl chloride. Computed intensities have been scaled to natural abundance (0.748937 for $CH_3{}^{35}Cl$ and 0.239491 for $CH_3{}^{37}Cl$) and are compared against all available lines in the HITRAN database. Overall the agreement is pleasing, particularly given the reduced size of the vibrational basis set and energy level thresholds. Up to 3200 cm^{-1} the only noticeable missing band in HITRAN appears to be the $2\nu_5$ band around 2880 cm^{-1}shown in Fig. 6. This is not expected to be important for atmospheric sensing.

An improved spectroscopic line list in the range 1900–2600 cm^{-1} was recently published [23] and considered transitions up to $J=47$ with absolute line intensities possessing an estimated uncertainty of 20% or less. In Fig. 7 a comparison of this region, which is composed of several weak bands, is shown for $CH_3{}^{35}Cl$. The DMS appears reasonable for much weaker intensities and the overall band structure in this region is well reproduced. There are some irregularities between TROVE and Nikitin et al. [23]; we expect that these are caused by the low-level nature of our calculations and also the assignment procedure in TROVE. In future work we intend to carry out a more comprehensive analysis of this region. Note that the computed

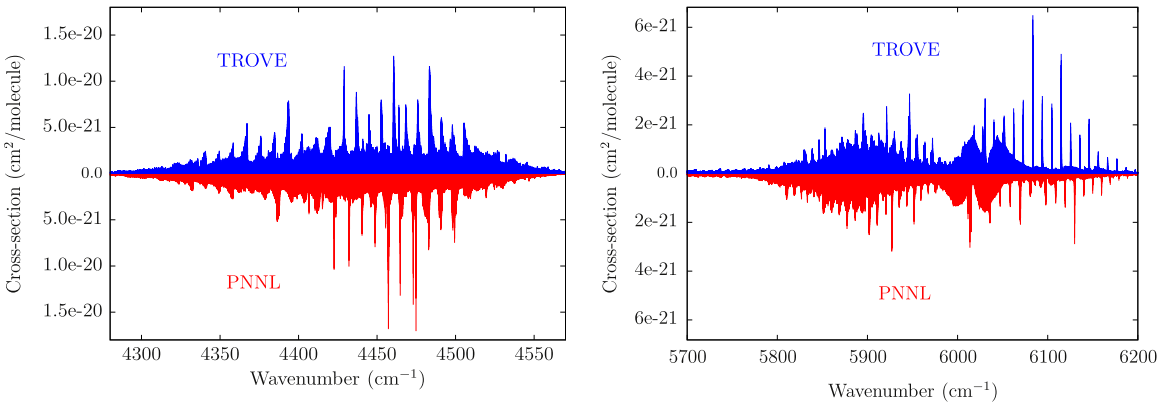

Fig. 8. Overview of simulated rotation–vibration spectrum in the 4300–4550 cm^{-1} (left) and 5700–6200 cm^{-1} (right) regions compared with the PNNL spectral library [34]. Computed intensities have been scaled to natural abundance.

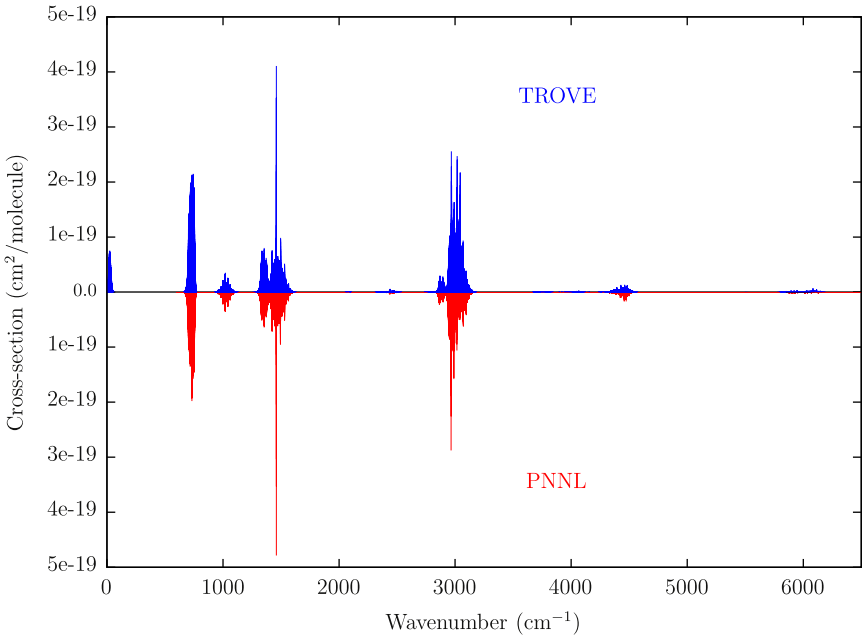

Fig. 9. Overview of methyl chloride rotation–vibration spectrum up to $J=85$ compared with the PNNL spectral library [34]. Computed intensities have been scaled to natural abundance.

TROVE line list has not been truncated at $J=47$ for this comparison.

Whilst spectral features above 3200 cm^{-1} are not as prominent there are noticeable bands between 4300–4550 cm^{-1} and 5700–6200 cm^{-1} as shown in Fig. 8. Here we have compared against the PNNL spectral library [34] (overview of entire spectrum presented in Fig. 9). Cross sections have been generated at a resolution of 0.06 cm^{-1} and fitted using a Gaussian profile with a half width at half maximum of 0.112 cm^{-1}. This line shape provides a straightforward and reasonable comparison [77], however, we expect that a Voigt profile dependent on instrumental factors would be more suitable.

Looking at Fig. 8 it is clear that our calculations are becoming worse at higher energies and producing spurious intensities. This is to be expected given the size of the vibrational basis set and thresholds imposed in our variational calculations. For the complete spectrum in Fig. 9 the agreement with PNNL is encouraging but does indicate the need for improved computations and line shape modelling.

5. Conclusions

A new nine-dimensional DMS for methyl chloride has been computed using high-level *ab initio* theory and fitted with a symmetry-adapted analytic representation. The DMS has been utilized to simulate the rotation–vibration spectrum of methyl chloride up to 6300 cm^{-1}. Overall, band shape and structure are well reproduced and there is good agreement with a range of experimental sources.

Notably, at least for fundamental bands that have been measured with high accuracy, computed absolute line intensities agree well with the available experimental data.

Considering the quality of the DMS and intensity simulations, further improvements could come from using a larger (augmented) basis set for the electronic structure calculations. However, this would be very computationally demanding and the change in predicted intensities may not necessarily reflect the computational effort. Empirical refinement of the PES [78] is expected to produce more reliable intensities [79] (as a result of better rovibrational energy levels and associated wavefunctions) and should thus be done when attempting to produce a line list suitable for high-resolution spectroscopy.

Most beneficial though will be improvements in the variational nuclear motion calculations. This will require increasing both the size of the vibrational basis set and the frequency range considered. Measurements of absolute line intensities of the order 10^{-26}–10^{-27} cm/molecule have been reported in the 11 590–11 760 cm^{-1} spectral region [26]. Presently we are unable to accurately model such high frequencies; this is a major challenge for variational calculations on small polyatomic molecules. We expect these issues to be addressed during the construction of a comprehensive, hot line list for inclusion in the ExoMol database [80,81].

Acknowledgements

The authors are grateful to Agnes Perrin and David Jacquemart for discussing results concerning their intensity measurements. This work was supported by ERC Advanced Investigator Project 267219, and FP7-MC-IEF project 629237.

Appendix A. Supplementary data

Supplementary data associated with this article can be found in the online version at http://dx.doi.org/10.1016/j.jqsrt.2016.06.037.

References

[1] Segura A, Kasting JF, Meadows V, Cohen M, Scalo J, Crisp D, et al. Biosignatures from Earth-like planets around M dwarfs. Astrobiology 2005;5:706–25. http://dx.doi.org/10.1089/ast.2005.5.706.

[2] Seager S, Bains W, Hu R. A biomass-based model to estimate the plausibility of exoplanet biosignature gases. Astrophys J 2013;775:104. http://dx.doi.org/10.1088/0004-637X/775/2/104.

[3] Seager S, Bains W, Hu R. Biosignature gases in H_2-dominated atmospheres on rocky exoplanets. Astrophys J 2013;777:95. http://dx.doi.org/10.1088/0004-637X/777/2/95.

[4] Bray C, Perrin A, Jacquemart D, Lacome N. The ν_1, ν_4 and $3\nu_6$ bands of methyl chloride in the 3.4-μm region: line positions and intensities. J Quant Spectrosc Radiat Transf 2011;112:2446–62. http://dx.doi.org/10.1016/j.jqsrt.2011.06.018.

[5] Bray C, Tran H, Jacquemart D, Lacome N. Line mixing in the ^{Q}Q sub branches of the ν_1 band of methyl chloride. J Quant Spectrosc Radiat Transf 2012;113:2182–8. http://dx.doi.org/10.1016/j.jqsrt.2012.07.026.

[6] Bray C, Jacquemart D, Buldyreva J, Lacome N, Perrin A. N_2 broadening coefficients of methyl chloride at room temperature. J Quant Spectrosc Radiat Transf 2012;113:1102–12. http://dx.doi.org/10.1016/j.jqsrt.2012.01.028.

[7] Bray C, Jacquemart D, Lacome N, Guinet M, Cuisset A, Eliet S, et al. Analysis of self-broadened pure rotational and rovibrational lines of methyl chloride at room temperature. J Quant Spectrosc Radiat Transf 2013;116:87–100. http://dx.doi.org/10.1016/j.jqsrt.2012.09.013.

[8] Bray C, Jacquemart D, Lacome N. Temperature dependence for self- and N_2-broadening coefficients of CH_3Cl. J Quant Spectrosc Radiat Transf 2013;129:186–92. http://dx.doi.org/10.1016/j.jqsrt.2013.06.013.

[9] Guinet M, Rohart F, Buldyreva J, Gupta V, Eliet S, Motiyenko RA, et al. Experimental studies by complementary terahertz techniques and semi-classical calculations of N_2 broadening coefficients of $CH_3{}^{35}Cl$. J Quant Spectrosc Radiat Transf 2012;113:1113–26. http://dx.doi.org/10.1016/j.jqsrt.2012.01.022.

[10] Buldyreva J, Guinet M, Eliet S, Hindle F, Mouret G, Bocquet R, et al. Theoretical and experimental studies of CH_3X-Y_2 rotational line shapes for atmospheric spectra modelling: application to room-temperature CH_3Cl-O_2. Phys Chem Chem Phys 2011;13:20326–34. http://dx.doi.org/10.1039/c1cp22232e.

[11] Buldyreva J, Rohart F. Experimental and theoretical studies of room-temperature sub-millimetre $CH_3{}^{35}Cl$ line shapes broadened by H_2. Mol Phys 2012;110:2043–53. http://dx.doi.org/10.1080/00268976.2012.684895.

[12] Buldyreva J. Air-broadening coefficients of $CH_3{}^{35}Cl$ and $CH_3{}^{37}Cl$ rovibrational lines and their temperature dependence by a semi-classical approach. J Quant Spectrosc Radiat Transf 2013;130:315–20. http://dx.doi.org/10.1016/j.jqsrt.2013.04.003.

[13] Buldyreva J, Margulès L, Motiyenko RA, Rohart F. Speed dependence of $CH_3{}^{35}Cl$-O_2 line-broadening parameters probed on rotational transitions: measurements and semi-classical calculations. J Quant Spectrosc Radiat Transf 2013;130:304–14. http://dx.doi.org/10.1016/j.jqsrt.2013.05.023.

[14] Barbouchi Ramchani A, Jacquemart D, Dhib M, Aroui H. Line positions, intensities and self-broadening coefficients for the ν_5 band of methyl chloride. J Quant Spectrosc Radiat Transf 2013;120:1–15. http://dx.doi.org/10.1016/j.jqsrt.2013.02.002.

[15] Barbouchi Ramchani A, Jacquemart D, Dhib M, Aroui H. Theoretical calculation of self-broadening coefficients for the ν_5 band of methyl chloride at various temperatures. J Quant Spectrosc Radiat Transf 2014;134:1–8. http://dx.doi.org/10.1016/j.jqsrt.2013.10.005.

[16] Ramchani AB, Jacquemart D, Dhib M, Aroui H. N_2 broadening coefficients of methyl chloride: measurements at room temperature and calculations at atmospheric temperatures. J Quant Spectrosc Radiat Transf 2014;148:186–96. http://dx.doi.org/10.1016/j.jqsrt.2014.07.008.

[17] Dudaryonok AS, Lavrentieva NN, Buldyreva JV. CH_3Cl self-broadening coefficients and their temperature dependence. J Quant Spectrosc Radiat Transf 2013;130:321–6. http://dx.doi.org/10.1016/j.jqsrt.2013.07.013.

[18] Dudaryonok AS, Lavrentieva NN, Buldyreva J, Margulès L, Motiyenko RA, Rohart F. Experimental studies, line-shape analysis and semi-empirical calculations of broadening coefficients for $CH_3{}^{35}Cl$-CO_2 submillimeter transitions. J Quant Spectrosc Radiat Transf 2014;145:50–6. http://dx.doi.org/10.1016/j.jqsrt.2014.04.015.

[19] Nikitin A, Féjard L, Champion JP, Bürger H, Litz M, Colmont JM, et al. New measurements and global analysis of chloromethane in the region from 0 to 1800 cm^{-1}. J Mol Spectrosc 2003;221:199–212. http://dx.doi.org/10.1016/S0022-2852(03)00221-2.

[20] Nikitin A, Champion JP, Bürger H. Global analysis of chloromethane: determinability of ground state constants. In: 14th Symposium on high-resolution molecular spectroscopy, SPIE proceedings, vol. 5311; 2004. p. 97–101, http://dx.doi.org/10.1117/12.545197.

[21] Nikitin A, Champion JP. New ground state constants of $^{12}CH_3{}^{35}Cl$ and $^{12}CH_3{}^{37}Cl$ from global polyad analysis. J Mol Spectrosc 2005;230:168–73. http://dx.doi.org/10.1016/j.jms.2004.11.012.

[22] Nikitin A, Champion JP, Bürger H. Global analysis of $^{12}CH_3{}^{35}Cl$ and $^{12}CH_3{}^{37}Cl$: simultaneous fit of the lower five polyads (0–2600 cm^{-1}). J Mol Spectrosc 2005;230:174–84. http://dx.doi.org/10.1016/j.jms.2004.11.012.

[23] Nikitin AV, Dmitrieva TA, Gordan IE. Improved spectroscopic line list of methyl chloride in the 1900–2600 cm^{-1} spectral region. J Quant Spectrosc Radiat Transf 2016;177:49–58. http://dx.doi.org/10.1016/j.jqsrt.2016.03.007.

[24] Gupta V, Rohart F, Margulès L, Motiyenko RA, Buldyreva J. Line-shapes and broadenings of rotational transitions of $CH_3{}^{35}Cl$ in collision with He, Ar and Kr. J Quant Spectrosc Radiat Transf 2015;161:85. http://dx.doi.org/10.1016/j.jqsrt.2015.03.032.

[25] Sahlberg A-L, Zhou J, Aldén M, Li ZS. Non-intrusive in situ detection of methyl chloride in hot gas flows using infrared degenerate four-

wave mixing. J Raman Spectrosc 2015;46:695. http://dx.doi.org/10.1002/jrs.4651.
[26] Lucchesini A, Gozzini S. Diode laser spectroscopy of methyl chloride overtones at 850–860 nm. J Quant Spectrosc Radiat Transf 2016;168:170. http://dx.doi.org/10.1016/j.jqsrt.2015.09.010.
[27] Wallington TJ, Pivesso BP, Lira AM, Anderson JE, Nielsen CJ, Andersen NH, et al. CH_3Cl, CH_2Cl_2, $CHCl_3$, and CCl_4: infrared spectra, radiative efficiencies, and global warming potentials. J Quant Spectrosc Radiat Transf 2016;174:56. http://dx.doi.org/10.1016/j.jqsrt.2016.01.029 ISSN 0022-4073.
[28] Nassar R, Bernath PF, Boone CD, Clerbaux C, Coheur PF, Dufour G, et al. A global inventory of stratospheric chlorine in 2004. J Geophys Res – Atmos. 2006;111:13. http://dx.doi.org/10.1029/2006JD007073.
[29] Brown AT, Chipperfield MP, Boone C, Wilson C, Walker KA, Bernath PF. Trends in atmospheric halogen containing gases since 2004. J Quant Spectrosc Radiat Transf 2011;112:2552–66. http://dx.doi.org/10.1016/j.jqsrt.2011.07.005.
[30] Brown AT, Volk CM, Schoeberl MR, Boone CD, Bernath PF. Stratospheric lifetimes of CFC-12, CCl_4, CH_4, CH_3Cl and N_2O from measurements made by the Atmospheric Chemistry Experiment-Fourier Transform Spectrometer (ACE-FTS). Atmos Chem Phys 2013;13:6921–50. http://dx.doi.org/10.5194/acp-13-6921-2013.
[31] Santee ML, Livesey NJ, Manney GL, Lambert A, Read WG. Methyl chloride from the Aura Microwave Limb Sounder: first global climatology and assessment of variability in the upper troposphere and stratosphere. J Geophys Res. – Atmos 2013;118:13532–60. http://dx.doi.org/10.1002/2013JD020235.
[32] Rothman L, Gordon I, Babikov Y, Barbe A, Benner DC, Bernath P, et al. The HITRAN2012 molecular spectroscopic database. J Quant Spectrosc Radiat Transf 2013;130:4–50. http://dx.doi.org/10.1016/j.jqsrt.2013.07.002.
[33] Kondo S, Koga Y, Nakanaga T. Infrared intensities in methyl chloride. III. Improvement of the anharmonic force field and the analysis of the overtone and combination band intensities. Bull Chem Soc Jpn 1985;58:65–72. http://dx.doi.org/10.1246/bcsj.58.65.
[34] Sharpe SW, Johnson TJ, Sams RL, Chu PM, Rhoderick GC, Johnson PA. Gas-phase databases for quantitative infrared spectroscopy. Appl Spectrosc 2004;58:1452–61. http://dx.doi.org/10.1366/0003702042641281.
[35] Jacquinet-Husson N, Crepeau L, Armante R, Boutammine C, Chédin A, Scott NA, et al. The 2009 edition of the GEISA spectroscopic database. J Quant Spectrosc Radiat Transf 2011;112:2395–445. http://dx.doi.org/10.1016/j.jqsrt.2011.06.004.
[36] Pickett HM, Poynter RL, Cohen EA, Delitsky ML, Pearson JC, Müller HSP. Submillimeter, millimeter, and microwave spectral line catalog. J Quant Spectrosc Radiat Transf 1998;60:883–90. http://dx.doi.org/10.1016/S0022-4073(98)00091-0.
[37] Margolis JS, Toth RA. Absorption strength measurement of the ν_1 band of methyl chloride. J Mol Spectrosc 1977;66:30–4. http://dx.doi.org/10.1016/0022–2852(77)90316–2.
[38] Margolis JS. Absorption strength of the perturbed ν_4 band of CH_3Cl. J Mol Spectrosc 1978;70:257–62. http://dx.doi.org/10.1016/0022–2852(78)90160–1.
[39] Dang-Nhu M, Morillon-Chapey M, Graner G, Guelachvili G. Intensities of the ν_1-bands of $^{12}CH_3{}^{35}Cl$ and $^{12}CH_3{}^{37}Cl$ near 3 μm. J Quant Spectrosc Radiat Transf 1981;26:515–21. http://dx.doi.org/10.1016/0022–4073(81)90038–8.
[40] Dang-Nhu M, Blanquet G, Walrand J, Derie F. Spectral intensities in the ν_3-band of $^{12}CH_3{}^{35}Cl$ at 13 μm. Mol Phys 1988;65:77–83. http://dx.doi.org/10.1080/00268978800100861.
[41] Elkins JW, Kagann RH, Sams RL. Infrared band strengths for methyl chloride in the regions of atmospheric interest. J Mol Spectrosc 1984;105:480–90. http://dx.doi.org/10.1016/0022-2852(84)90235-2.
[42] Cappellani F, Restelli G, Tarrago G. Absolute infrared intensities in the fundamentals ν_2 and ν_5 of $^{12}CH_3{}^{35}Cl$. J Mol Spectrosc 1991;146:326–33. http://dx.doi.org/10.1016/0022–2852(91)90007-W.
[43] Blanquet G, Walrand J, Dang-Nhu M. Spectral intensities in the ν_3 band of $^{12}CH_3{}^{37}Cl$. J Mol Spectrosc 1989;133:471–4. http://dx.doi.org/10.1016/0022–2852(89)90207–5.
[44] Blanquet G, Walrand J, Dang-Nhu M. Absolute line intensities of the ν_6 band of $CH_3{}^{35}Cl$ at 10 μm. J Mol Spectrosc 1993;159:156–60. http://dx.doi.org/10.1006/jmsp.1993.1114.
[45] Blanquet G, Walrand J, Dang-Nhu M. Intensities of the ν_6 band of $^{12}CH_3{}^{37}Cl$ at 10 μm. J Mol Spectrosc 1993;162:513–5. http://dx.doi.org/10.1006/jmsp.1993.1303.
[46] Bouanich JP, Blanquet G, Walrand J. Diode-laser measurements of self-broadening coefficients and line strengths in the ν_3 band of $CH_3{}^{35}Cl$. J Quant Spectrosc Radiat Transf 1994;51:573–8. http://dx.doi.org/10.1016/0022-4073(94)90111-2.
[47] Blanquet G, Coupe P, Walrand J, Bouanich JP. Determination of broadening coefficients and intensities for overlapping spectral lines with application to the $^{Q}R(3,K)$ lines in the ν_3 band of $CH_3{}^{35}Cl$. J Quant Spectrosc Radiat Transf 1994;51:671–8. http://dx.doi.org/10.1016/0022-4073(94)90123-6.
[48] Blanquet G, Walrand J, Populaire JC, Bouanich JP. Self-broadening coefficients and line strengths in the ν_3 band of $CH_3{}^{35}Cl$ at low temperature. J Quant Spectrosc Radiat Transf 1995;53:211–9. http://dx.doi.org/10.1016/0022-4073(95)90008-X.
[49] Blanquet G, Lance B, Walrand J, Bouanich JP. Absolute line intensities in the ν_2 band of $^{12}CH_3{}^{35}Cl$ at 7.5 μm. J Mol Spectrosc 1995;170:466–77. http://dx.doi.org/10.1006/jmsp.1995.1085.
[50] Blanquet G, Lance B, Walrand J, Bouanich JP. Absolute line intensities in the ν_2 band of $^{12}CH_3{}^{35}Cl$ at 7.5 μm. Spectrochim Acta, Part A 1996;52:1033–5. http://dx.doi.org/10.1016/0584-8539(95)01610-4.
[51] Wiberg KB. Infrared intensities. The methyl halides. Effect of substituents on charge distributions. J Am Chem Soc 1979;101:1718–22. http://dx.doi.org/10.1021/ja00501a012.
[52] Kondo S, Koga Y, Nakanaga T, Saëki S. Infrared intensities in methyl chloride. I. The fundamental bands. Bull Chem Soc Jpn 1983;56:416–21. http://dx.doi.org/10.1246/bcsj.56.416.
[53] Kondo S, Koga Y, Nakanaga T, Saëki S. Infrared intensities in methyl chloride. II. Binary overtone and combination bands. Bull Chem Soc Jpn 1984;57:16–21. http://dx.doi.org/10.1246/bcsj.57.16.
[54] Schneider W, Thiel W. Ab initio calculation of harmonic force fields and vibrational spectra for the methyl, silyl, germyl, and stannyl halides. J Chem Phys 1987;86:923–36. http://dx.doi.org/10.1063/1.452239.
[55] Chong DP, Papoušek D. Electric dipole moment derivatives for PH_3, PD_3, CH_3F, CD_3F, CH_3Cl, and CD_3Cl computed by the density functional method. J Mol Spectrosc 1992;155:167–76. http://dx.doi.org/10.1016/0022-2852(92)90556-4 ISSN 0022-2852.
[56] Papoušek D, Papoušková Z, Chong DP. Density functional computations of the dipole moment derivatives for halogenated methanes. J Phys Chem 1995;99:15387–95. http://dx.doi.org/10.1021/j100042a010.
[57] Jalbout AF, Trzaskowski B, Xia Y, Li Y. Geometry predictions, vibrational analysis and IR intensities of XH_3Y (X=C, Si, Ge, Y=F, Cl, Br) calculated by hybrid density functional theory, MP2 and MP4 methods. Acta Chim Slov 2007;54:769–77.
[58] Owens A, Yurchenko SN, Yachmenev A, Tennyson J, Thiel W. Accurate ab initio vibrational energies of methyl chloride. J Chem Phys 2015;142:244306. http://dx.doi.org/10.1063/1.4922890.
[59] Yurchenko SN, Thiel W, Jensen P. Theoretical ROVibrational Energies (TROVE): a robust numerical approach to the calculation of rovibrational energies for polyatomic molecules. J Mol Spectrosc 2007;245:126–40. http://dx.doi.org/10.1016/j.jms.2007.07.009.
[60] Dunning Jr. TH. Gaussian basis sets for use in correlated molecular calculations. 1. The atoms boron through neon and hydrogen. J Chem Phys 1989;90:1007. http://dx.doi.org/10.1063/1.456153.
[61] Kendall RA, Dunning Jr. TH, Harrison RJ. Electron affinities of the first-row atoms revisited. Systematic basis sets and wave functions. J Chem Phys 1992;96:6796–806. http://dx.doi.org/10.1063/1.462569.
[62] Woon DE, Dunning Jr. TH. Gaussian basis sets for use in correlated molecular calculations. III. The atoms aluminum through argon. J Chem Phys 1993;98:1358–71. http://dx.doi.org/10.1063/1.464303.
[63] Dunning Jr. TH, Peterson KA, Wilson AK. Gaussian basis sets for use in correlated molecular calculations. X. The atoms aluminum through argon revisited. J Chem Phys 2001;114:9244. http://dx.doi.org/10.1063/1.1367373.
[64] Werner H-J, Knowles PJ, Knizia G, Manby FR, Schütz M. Molpro: a general-purpose quantum chemistry program package. WIREs Comput Mol Sci 2012;2:242–53. http://dx.doi.org/10.1002/wcms.82.
[65] Bunker PR, Jensen P. Molecular symmetry and spectroscopy. 2nd ed. Ottawa: NRC Research Press; 1998.
[66] Yurchenko SN, Barber RJ, Yachmenev A, Thiel W, Jensen P, Tennyson J. A variationally computed $T=300$ K line list for NH_3. J Phys Chem A 2009;113:11845–55. http://dx.doi.org/10.1021/jp9029425.
[67] Underwood DS, Tennyson J, Yurchenko SN. An ab initio variationally computed room-temperature line list for $^{32}S^{16}O_3$. Phys Chem Chem Phys 2013;15:10118–25. http://dx.doi.org/10.1039/c3cp50303h.
[68] Watson JKG. Robust weighting in least-squares fits. J Mol Spectrosc 2003;219:326–8. http://dx.doi.org/10.1016/S0022-2852(03)00100-0.
[69] Partridge H, Schwenke DW. The determination of an accurate isotope dependent potential energy surface for water from extensive ab initio calculations and experimental data. J Chem Phys 1997;106:4618–39. http://dx.doi.org/10.1063/1.473987.

[70] Lee TJ, Taylor PR. A diagnostic for determining the quality of single-reference electron correlation methods. Int J Quantum Chem 1989;36:199–207. http://dx.doi.org/10.1002/qua.560360824.
[71] Yachmenev A, Yurchenko SN. Automatic differentiation method for numerical construction of the rotational-vibrational Hamiltonian as a power series in the curvilinear internal coordinates using the Eckart frame. J Chem Phys 2015;143:014105. http://dx.doi.org/10.1063/1.4923039.
[72] Wlodarczak G, Segard B, Legrand J, Demaison J. The dipole moment of $CH_3{}^{35}Cl$. J Mol Spectrosc 1985;111:204–6. http://dx.doi.org/10.1016/0022–2852(85)90083–9.
[73] Owens A, Yurchenko SN, Yachmenev A, Thiel W. A global potential energy surface and dipole moment surface for silane. J Chem Phys 2015;143:244317. http://dx.doi.org/10.1063/1.4938563.
[74] Jensen P, Bunker PR. Nuclear spin statistical weights revisited. Mol Phys 1999;97:821–4. http://dx.doi.org/10.1080/00268979909482882.
[75] Jacquemart D, Perrin A. Private communication; 2016.
[76] Šimečkova M, Jacquemart D, Rothman LS, Gamache RR, Goldman A. Einstein A-coefficients and statistical weights for molecular absorption transitions in the HITRAN database. J Quant Spectrosc Radiat Transf 2006;98:130–55. http://dx.doi.org/10.1016/j.jqrst.2005.07.003.
[77] Al-Refaie AF, Yachmenev A, Tennyson J, Yurchenko SN. ExoMol line lists VIII: a variationally computed line list for hot formaldehyde. Mon Not R Astron Soc 2015;448:1704–14. http://dx.doi.org/10.1093/mnras/stv091.
[78] Yurchenko SN, Barber RJ, Tennyson J, Thiel W, Jensen P. Towards efficient refinement of molecular potential energy surfaces: ammonia as a case study. J Mol Spectrosc 2011;268:123–9. http://dx.doi.org/10.1016/j.jms.2011.04.005.
[79] Ovsyannikov RI, Thiel W, Yurchenko SN, Carvajal M, Jensen P. PH_3 revisited: theoretical transition moments for the vibrational transitions below 7000 cm^{-1}. J Mol Spectrosc 2008;252:121–8. http://dx.doi.org/10.1016/j.jms.2008.07.005.
[80] Tennyson J, Yurchenko SN. ExoMol: molecular line lists for exoplanet and other atmospheres. Mon Not R Astron Soc 2012;425:21–33. http://dx.doi.org/10.1111/j.1365–2966.2012.21440.x.
[81] Tennyson J, Yurchenko SN, Al-Refaie AF, Barton EJ, Chubb KL, Coles PA, et al. The ExoMol database: molecular line lists for exoplanet and other hot atmospheres. J Mol Spectrosc; 2016, http://dx.doi.org/10.1016/j.jms.2016.05.002.